Structural and electrical properties under high pressure for the superconducting spin-ladder system $Sr_{0.4}Ca_{13.6}Cu_{24}O_{41+\delta}$

M. Isobe, T. Ohta, M. Onoda, F. Izumi, S. Nakano, J. Q. Li,* Y. Matsui, and E. Takayama-Muromachi

National Institute for Research in Inorganic Materials (NIRIM), 1-1 Namiki, Tsukuba, Ibaraki 305 Japan

T. Matsumoto

National Research Institute for Metals (NRIM), 1-2-1 Sengen, Tsukuba, Ibaraki 305 Japan

H. Hayakawa

National Institute of Materials and Chemical Research (NIMC), 1-1 Higashi, Tsukuba, Ibaraki 305 Japan

(Received 23 June 1997)

We studied structural and electrical properties under high pressure and low temperature for a $S = 1/2$ Heisenberg two-leg ladder compound $Sr_{0.4}Ca_{13.6}Cu_{24}O_{41+\delta}$. It showed a superconducting transition above 3 GPa with a maximum T_c of 13 K. The $Sr_{0.4}Ca_{13.6}Cu_{24}O_{41+\delta}$ phase survives at least up to 9 GPa and down to 7 K without decomposition or phase transition, indicating that it is responsible for the observed superconductivity. The most important role of high pressure for realizing superconductivity is enhancement of the interaction between the Cu_2O_3 ladder and the one-dimensional CuO_2 chain which accelerates redistribution of holes via locally formed Cu_{ladder}-O_{chain} hybrid orbitals. Electrical property of the normal state is affected by the carrier density, dimensionality, random potential, and spin scattering which are related to structural modification under high pressure. [S0163-1829(98)08201-0]

I. INTRODUCTION

Recently, so-called spin-ladder systems have attracted many researchers' attention. They consist of even or odd numbers of antiferromagnetic one-dimensional (1D) Heisenberg chains (legs) which are connected by rungs. A finite energy gap was predicted theoretically for a magnetic excitation in the even-leg ladder system from $S = 0$ spin singlet ground states to $S = 1$ triplet states.[1] The presence of the spin gap was verified by dc magnetic-susceptibility measurements, inelastic neutron scattering, and NMR experiments for $(VO)_2P_2O_7$ (Refs. 2–4) and $SrCu_2O_3$.[5–7] The latter is a Cu-based two-leg ladder phase stable under high pressure.[5] A more exciting prediction is the appearance of "d-wave" superconductivity in an even-leg ladder system doped with hole carriers. According to various calculations for the two-leg spin ladder,[1,8–21] it is energetically favorable at low temperature for carriers to form singlet pairs leading to superconducting or charge-density-wave (CDW) states. Separation between spin and charge would occur in such a system,[22] and the gap for spin excitation survives for a certain range of doping level but that for charge excitation vanishes, resulting in a magnetically correlated metallic phase.

Stimulated by the theoretical prediction, tremendous efforts have been made to realize superconductivity in even-leg materials. However, carrier doping for a ladder system is generally difficult and it was not successful for $SrCu_2O_3$. Systematic hole doping into the two-leg ladder phase was achieved by Hiroi *et al.* in $LaCuO_{2.5}$ by substituting Sr for La.[23–25] This material exhibits an insulator-to-metal transition with increasing the Sr content but no sign of superconductivity was observed. In carrier doping by the partial substitution of heterovalence ions, random potential is inevitably induced and it often has serious effects in a low-dimensional material such as the ladder system.

$(Sr,Ca)_{14}Cu_{24+y}O_{41+\delta}$ is a composite crystal which consists of two interpenetrated subsystems (Fig. 1).[26–32] The first subsystem $[(Sr,Ca)_2Cu_2O_3]$ is composed of $(Cu_2O_3)_\infty$ sheets of two-leg ladders and (Sr,Ca) ions coordinated to them. In the second subsystem, CuO_4 squares are connected by edge-sharing forming 1D $(CuO_2)_\infty$ chains running along the c axis. The 1D chains are sandwiched by the (Sr,Ca) planes of the first subsystem. The atomic positions are modulated incommensurately due to interaction between the two subsystems. $(Sr,Ca)_{14}Cu_{24+y}O_{41+\delta}$ has two types of spin gaps corresponding to spin excitations in the 1D chains and in the ladders.[33–35] An interesting aspect of this compound is "self doping" of holes, i.e., about six holes exist already per a
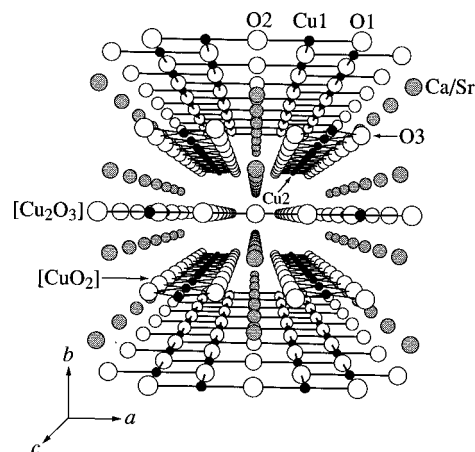

FIG. 1. Idealized crystal structure of $(Sr,Ca)_{14}Cu_{24+y}O_{41+\delta}$ viewed in perspective along the c direction.

molecule without substitution.

Though $Sr_{14}Cu_{24+y}O_{41+\delta}$ shows semiconducting behavior, resistivity decreases with Ca substitution for Sr.[36–39] Recently, Uehara *et al.* succeeded in preparing a highly Ca-substituted phase $Sr_{0.4}Ca_{13.6}Cu_{24}O_{41.84}$ under high oxygen pressure and reported that it shows superconductivity with the maximum T_c of 12 K near 3 GPa.[40] Their sensational report seems to prove the theoretical prediction on the spin-ladder system. In addition, it may give insights for the mechanism of superconductivity in 2D high-T_c cuprates. However, superconductivity in $Sr_{0.4}Ca_{13.6}Cu_{24}O_{41.84}$ is observed only under high pressure and there are still various problems to be solved. In particular, we have little information about its structural properties under high pressure. It is a key for understanding the role of high pressure to know pressure-induced structural changes. In the present study, we performed x-ray-diffraction and electrical resistivity measurements under high pressure and low temperature. The results are discussed in relation to the possibility of structural phase transition, carrier doping mechanisms, effects of dimensionality, and electronic structure.

II. EXPERIMENT

Starting materials of $SrCO_3(99.9\%)$, $CaCO_3(99.9\%)$, and $CuO(99.9\%)$ were mixed in an agate mortar and calcined at 950 °C for over 4 days in air with several intermediate grindings, to obtain a multiphase mixture having a net composition of $Sr_{0.4}Ca_{13.6}Cu_{24}O_z$. It was heated at 1200 °C for 24 h in Ar-based 20% O_2 mixture gas at $P_{total} = 2000$ kg f/cm² using a hot-isostatic-press (HIP) apparatus. A single-phase sample of $Sr_{0.4}Ca_{13.6}Cu_{24+y}O_{41+\delta}$ was obtained through this process at least judging from its x-ray pattern.

Powder x-ray-diffraction patterns at ambient pressure and room temperature (XRD) were obtained by a diffractometer (Philips PW-1800) equipped with a Cu $K\alpha$ x-ray source, a curved graphite monochrometer on the counter side and an auto-divergence-slit system. Low-temperature x-ray-diffraction patterns under ambient pressure (LT-XRD) were measured down to 10 K at NIMC using a diffractometer (MAC science, MXP system) with a Cu $K\alpha$ x-ray source and a closed-cycle He refrigerator. Si powder (NBS 640b) was used as an internal standard; its lattice constant at low temperature was calculated based on the thermal-expansion data.[41] Lattice constants of the $Sr_{0.4}Ca_{13.6}Cu_{24+y}O_{41+\delta}$ phase were calculated by the least-squares method for more than 50 Bragg's reflections between $2\theta = 28-80°$.

High-pressure x-ray-diffraction patterns at room-temperature (HP-XRD) were obtained by the Debye-Scherrer method using a diamond-anvil cell combined with Mo $K\alpha$ x-ray source, a graphite monochrometer, and an imaging-plate (IP) detector. A small amount of sample was placed in a SUS304 gasket with the pressure-transmitting fluid, a mixture of methanol-ethanol at a volume ratio of 4:1. Pressure was measured on several points in the sample space by the ruby fluorescence method based on previous scale data.[42] From the Debye-Scherrer pattern on the IP, an usual 2θ pattern was obtained by integrating the raw intensity data along the Debye-Scherrer ring.

X-ray-diffraction patterns at high pressure and low temperature (HPLT-XRD) were obtained at NRIM using the cubic-anvil-type high-pressure apparatus for measuring physical properties (CAHP) equipped with six tungsten carbide anvil tops having a square face of 4×4 mm². The powder form of the sample was mixed with polyethylene and was filled in a gasket made of amorphous boron and epoxy resin at a ratio of 4:1. In order to keep the pressure constant during a heat cycle, the load applied to the system was controlled to be constant. The pressure was calibrated by comparing the observed lattice constant of NaCl with the calculated one.[43] The x-ray source beam was a white radiation from a table-top-type W anode. The diffraction beam was detected by a solid-state detector through the collimators with a fixed diffraction angle of $2\theta = 11°$. The energy-dispersive data were numerically converted to angle dispersive ones corresponding to the Cu $K\alpha$ radiation.[44]

Electrical resistivity under high pressure and low temperature was measured by the standard four-probe dc method using the CAHP. A $1.55\times0.50\times0.45$ mm³ bulk sample was placed in a teflon cell with the fluid pressure-transmitting medium, a mixture of Fluorinate FC70 and FC77. The cell was buried in the gasket. The tungsten carbide anvil tops with a square face of 6×6 mm² were used instead of the 4 $\times4$ mm² ones. Electron-diffraction (ED) experiments were carried out by a high-resolution transmission electron microscopy (Hitachi H-1500) operated at 800 kV.[45]

III. RESULTS

Measurement of ED patterns is an effective way to know a crystal symmetry and to assign an x-ray pattern. There are several reports of the ED patterns for Ca-poor $(Sr,Ca)_{14}Cu_{24+y}O_{41+\delta}$ samples[46–48] but little data are available on the Ca-rich superconducting phase. The ED patterns of $Sr_{0.4}Ca_{13.6}Cu_{24+y}O_{41+\delta}$ obtained in the present study are shown in Figs. 2(a) and 2(b), for a^*-b^* and b^*-c^* sections, respectively. These patterns are consistent with a composite structure and the reciprocal space is regarded as consisting of two orthorhombic sublattices. The sublattices have common a^* and b^* axes but different c^* ones, c_1^* corresponding to the $[(Sr,Ca)_2Cu_2O_3]$ subsystem and c_2^* to $[CuO_2]$. In this paper, we define the a axis as the rung direction and the b axis as the interlayer direction (see Fig. 1).

A reciprocal-lattice vector $\mathbf{q}$ is expressed by a set of four integers (h,k,l,m) in a formula, $\mathbf{q} = h\mathbf{a}^* + k\mathbf{b}^* + l\mathbf{c}_1^* + m\mathbf{c}_2^*$.[49,50] In Fig. 2(b), weak first-order satellite peaks with $l\neq0$ and $m\neq0$ are seen around the fundamental spots with $l=0$ and/or $m=0$. These satellites are attributed to the deviation from the average structure due to the interaction between the subsystems. From the systematic reflection conditions for fundamental spots: $h+k=2n$, $k+l=2n$, and $l+h=2n$ for $hkl0$; $h+k=2n$, $k+m=2n$, and $m+h=2n$ for $hk0m$, it was found that the each subsystem has the same symmetry on basic structures with a space group of $Fmm2$, $F222$ or $Fmmm$. The present ED patterns are essentially the same as those reported for the Ca-poor samples.[26,28–29,31,46]

The crystal structure of the present $Sr_{0.4}Ca_{13.6}Cu_{24+y}O_{41+\delta}$ sample was determined by a combined neutron and x-ray Rietveld refinement using a super-space group approach; detailed results will be published
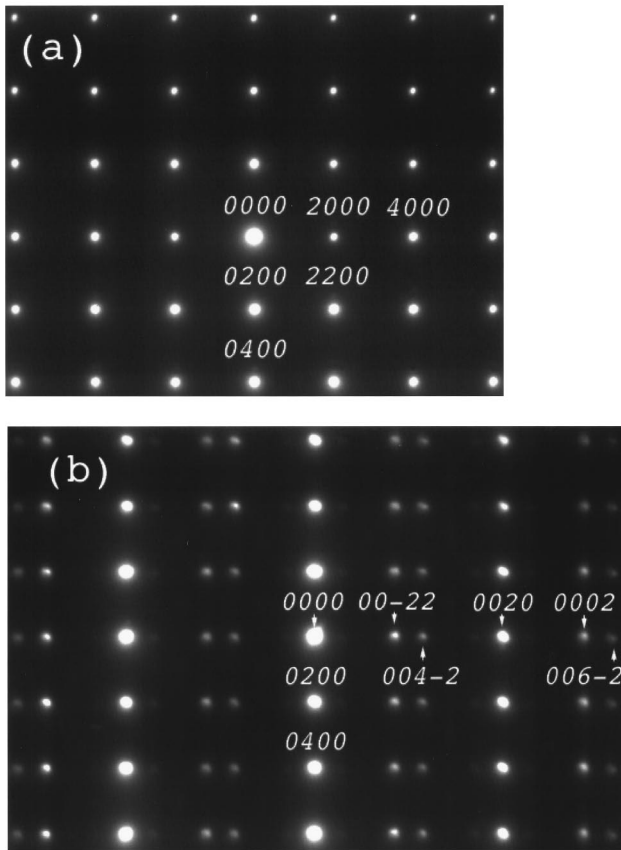
FIG. 2. Electron-diffraction patterns of $Sr_{0.4}Ca_{13.6}Cu_{24+y}O_{41+\delta}$ for (a) a^*-b^* and (b) b^*-c^* sections.

FIG. 4. Low-temperature x-ray-diffraction patterns under ambient pressure.

elsewhere.[51] According to the refinement, lattice parameters were $a = 11.260\ 78(1)$ Å, $b = 12.426\ 66(2)$ Å, $c_1 = 3.904\ 911(6)$ Å, and $c_2 = 2.738\ 21$ Å: $c_1/c_2 = 1.426\ 08(1)$. The c_1/c_2 is closed to 10/7 ($=1.428\ 57$) within the mismatch of $\sim 0.18\%$, indicating that the chemical formula of the compound can be approximately expressed as $Sr_{0.4}Ca_{13.6}Cu_{24}O_{41+\delta}$ ($y=0$). Hereafter, we regard this phase as a commensurate one with $c = 7c_1 = 10c_2$ and call it "14-24."

Figure 3 shows an x-ray pattern of the 14-24 phase at ambient pressure and room temperature. All diffraction peaks were assigned using the four integers. There is only one satellite reflection of $22\bar{1}1$ near $2\theta = 23°$. Figure 4
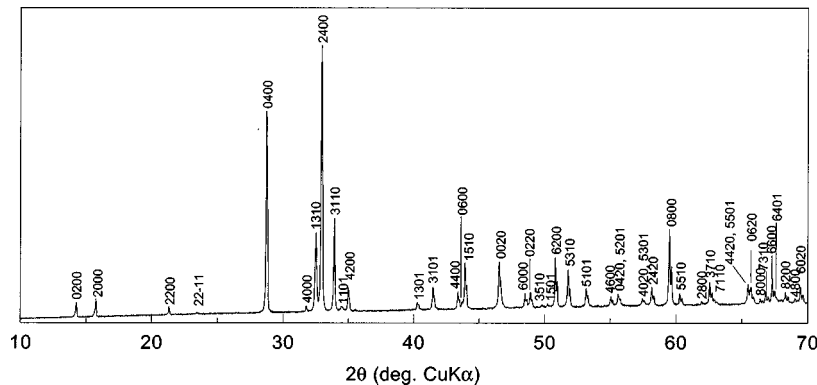
shows LT-XRD data under ambient pressure for some selected temperatures. The diffraction pattern was essentially kept unchanging between 10 and 298 K and the 14-24 structure survives for the entire range of temperature. We inspected very carefully the profile shape of each peak but no peak splittings were detected for the entire range of temperature. Moreover, the peak shifts due to thermal expansion (or shrinkage) were completely reversible for a cyclic change of temperature.

The lattice constants are plotted in Fig. 5 as functions of temperature. The lattice shrinks anisotropically from 298 to 10 K in 0.036, 0.33, and 0.090% for the a, b, and c axis, respectively. The c axis slightly shrinks with decreasing temperature, whereas the a axis is almost constant in the entire range of temperature. The b axis changes in proportion to temperature between 200 and 300 K, and its shrinkage saturates below 100 K. It is noted that an anomalous change of the b axis was observed around 150 K, suggesting a singularity in the thermal lattice expansivity.

HP-XRD patterns at room-temperature are shown in Fig. 6. The pressure was induced from 0.15 to 9.1 GPa, then released to 2.1 GPa. In a preliminary experiment, we confirmed reversible change in the x-ray pattern for cyclic change of pressure. Almost all reflection peaks in each dif-

FIG. 3. A powder x-ray-diffraction pattern of $Sr_{0.4}Ca_{13.6}Cu_{24}O_{41+\delta}$ at ambient pressure and room temperature.
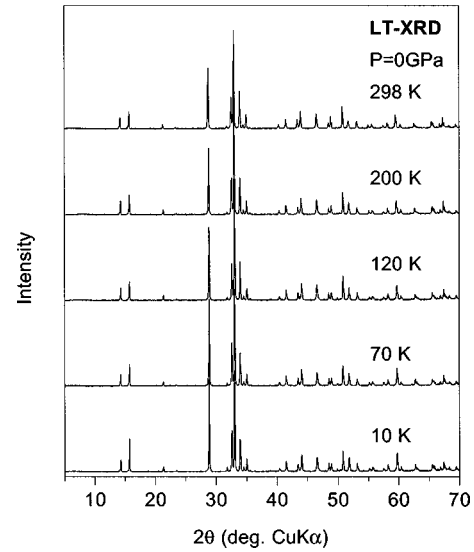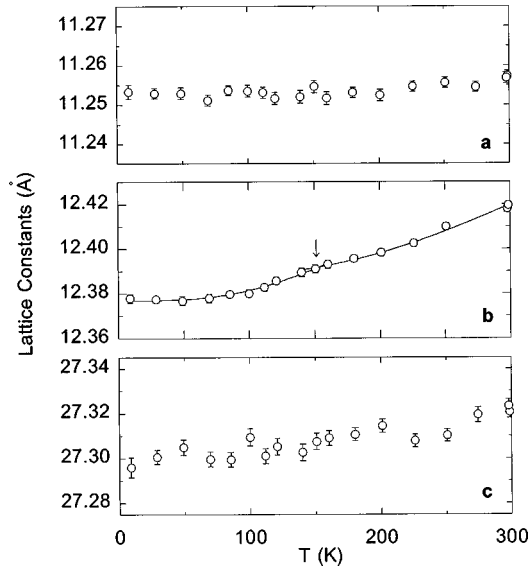
FIG. 5. The temperature variation of the lattice constants under ambient pressure. The arrow indicates an anomalous change of the *b* axis (see text).

fraction pattern could be assigned on the basis of the 14-24 structure. In addition, there are no significant changes in the peak profile upon increasing pressure except for the peak shift due to the lattice compression and slight peak broadening probably due to inhomogeneity in pressure. One weak extra peak appears around $2\theta = 17°$ above 3 GPa (see arrows in Fig. 6). This peak grows with increasing pressure and disappears reversibly when the pressure was released to 2.1 GPa.

The compression of the lattice parameters up to 7 GPa is shown in Fig. 7. We can see there a remarkable anisotropy of the compression. The *b* axis largely shrinks in 0.73% per 1 GPa, while the *a* axis is almost constant for the entire range of pressure examined. It indicates hard intraplane binding and soft interplane one. The percent shrinkages per 1 GPa are summarized in Table I for the three axes and the cell
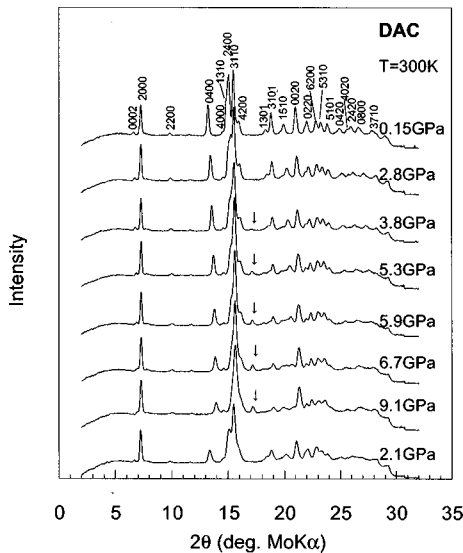

FIG. 6. High-pressure x-ray-diffraction patterns at room temperature. A weak extra peak around $2\theta = 17°$ is shown by an arrow.
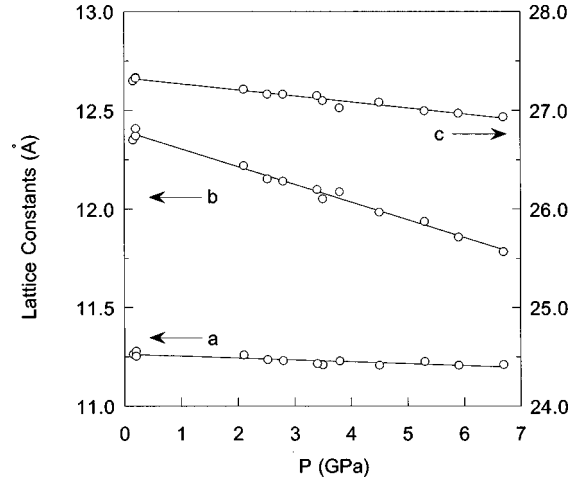

FIG. 7. Pressure variation of the lattice constants.

volume. The lattice also shrinks by replacement of Ca for Sr ("chemical pressure"). We calculated the percent shrinkages per the Ca content *x* in $Sr_{14-x}Ca_xCu_{24}O_{41+\delta}$ from the changes of the lattice constants in the samples with $x = 13.0$–13.8; the results are listed in Table I. (Though the sample with a nominal composition of $Sr_{0.2}Ca_{13.8}Cu_{24}O_{41+\delta}$ contains a small amount of impurity phase(s), the lattice constants of the 14-24 phase change linearly with the Ca content *x* up to $x = 13.8$.) If we compare the data for the cell volume, increase of pressure by 1 GPa corresponds to an increase of the Ca content by 1.22.

HPLT-XRD patterns are shown in Fig. 8. The overall x-ray pattern does not change noticeably, i.e., the 14-24 structure is stable under high pressure and low temperature, in particular, at 5 GPa and 7 K, where the system is in the superconducting state (see below). The extra peak observed by the HP-XRD also appeared below 10 K but its intensity is minimal (see arrow in Fig. 8).

The temperature dependences of the lattice constants are plotted in Fig. 9 for 1.9, 5, and 7 GPa. The *b* and *c* axis shrink with decreasing temperature at every pressure. The temperature dependence of the *a* axis is worth noting. As described above, the *a* axis is almost independent of temperature under ambient pressure. However, the thermal shrinkage is far more pronounced at 7 GPa. Namely, the *a* axis shrinks substantially under high-pressure and low-temperature region.

Figure 10 shows the temperature dependence of the electrical resistivities under various pressures of 0–6 GPa. The

TABLE I. The percent shrinkages of each axis and the cell volume per 1 GPa in $Sr_{0.4}Ca_{13.6}Cu_{24}O_{41+\delta}$, and those per Ca content *x* in $Sr_{14-x}Ca_xCu_{24}O_{41+\delta}$.

	Pressure	Ca substitution[a]	*x* corresponding to 1 GPa
a axis	0.08%	0.14%	0.60
b axis	0.73%	0.59%	1.24
c axis	0.22%	0.10%	2.13
Cell volume	1.02%	0.83%	1.22

[a]The values were obtained from the changes of the lattice constants in the samples with $x = 13.0$–13.8.
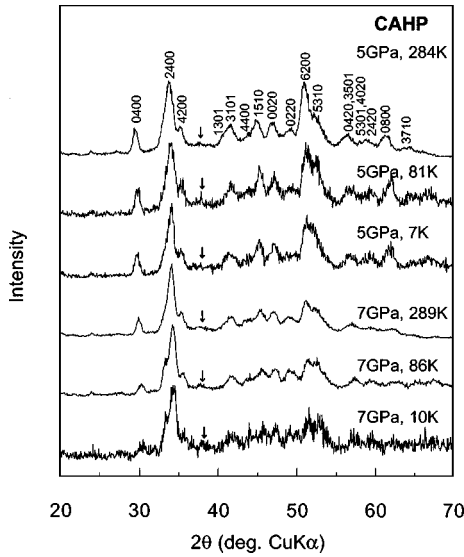
FIG. 8. High-pressure x-ray diffraction patterns at various temperatures. The weak extra peak is shown by an arrow.

results are essentially identical with those reported by Uehara *et al.*[40] We can see the successive change of the resistivity curves with increasing pressure. At ambient pressure, the ρ-T curve has a broad hump between 160 and 50 K, i.e., there exist two metal-semiconductor-like transitions at ~ 160 and ~ 50 K. As pressure increases, the hump reduces accompanying decrease of the resistivity. The hump disappears above 5 GPa and the sample goes into metallic regime. The resistivity at room temperature is shown as a function of pressure in Fig. 11, which shows almost linear temperature dependence. Superconducting transition appeared around 9 K at 3 GPa. The T_c^{onset} is plotted against the pressure in Fig. 12. It increases with pressure and reaches the maximum of ~ 13 K at 5 GPa, then reduces. T_c of the present phase is lower than those of 2D high-T_c cuprates but is much higher than those of typical metal superconductors in spite of its low carrier density. It implies an exotic pairing mechanism in the ladder compound.
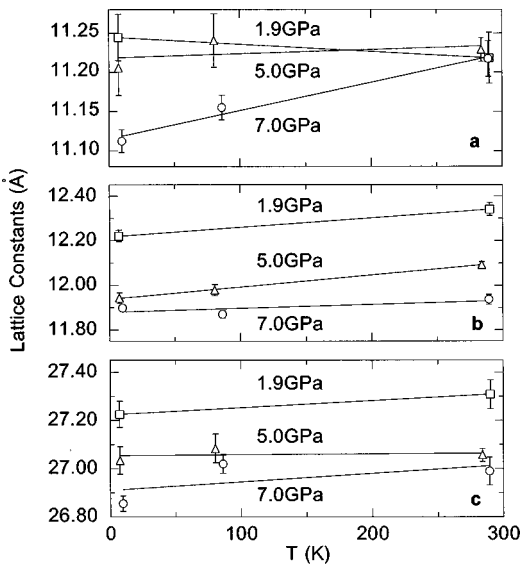

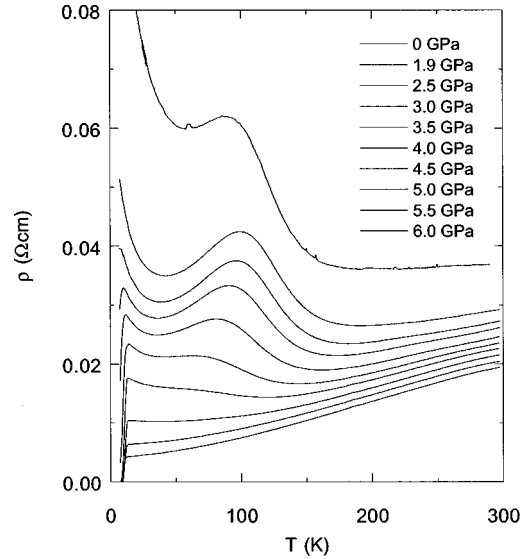FIG. 9. Temperature variation of the lattice constants at 1.9, 5, and 7 GPa.

FIG. 10. Temperature dependence of the electrical resistivities at various pressures.

IV. DISCUSSION

The first question to be answered is if the 14-24 phase is really responsible for superconductivity which is observed only under high pressure. Our LT-, HP-, and LTHP-XRD data indicates clearly that the 14-24 phase survives under the high-pressure and low-temperature region. Besides the peak shifts due to the lattice shrinkage, the appearance of a weak additional diffraction peak near $2\theta = 17°$ was only a substantial change in the XRD pattern under high pressure (Fig. 6). However, it is unlikely that this peak is due to a secondary phase formed through phase transition or decomposition of the 14-24 phase because the peak intensity changes smoothly and reversibly as a function of pressure. This peak may be a higher-order satellite since its peak position can be explained assuming $04\bar{2}2$ reflection; some structural modification may occur under high pressure which enhances such a higher-order satellite reflection. The origin of the extra peak is not clear yet. Nevertheless, it does not cast serious doubt that the 14-24 phase is responsible for superconductivity. The peak intensity increases monotonously with pressure at least up to
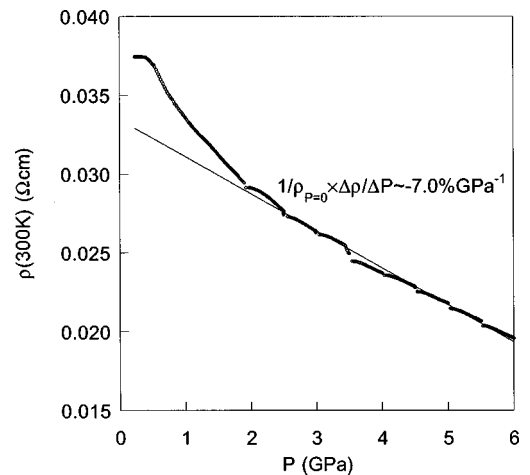

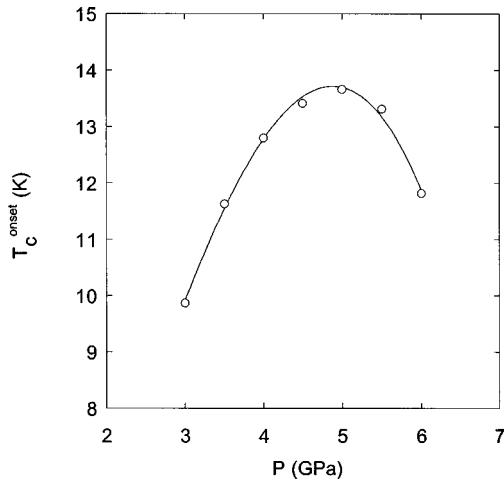FIG. 11. Pressure variation of the resistivity at room temperature.

FIG. 12. Variation of T_c^{onset} as a function of pressure.

9.1 GPa regardless of suppression of superconductivity above 5 GPa. Also, its intensity around 3.8 GPa seems too small to explain bulk superconductivity.

A second question is the role of high pressure for superconductivity. To answer this question, it is worth noting structural changes induced by the Ca substitution for Sr (increase of x in $Sr_{14-x}Ca_xCu_{24}O_{41+\delta}$), since the Ca substitution has similar, though not equivalent, effects on the lattice as does high pressure (see Table I). According to the detailed structure analysis on the present Ca-rich phase,[51] the most drastic change after the Ca substitution is enhancement of the interaction between the ladder and the 1D chain subsystems. The minimum interatomic distance between Cu_{ladder}-O_{chain} becomes ~ 2.7 Å in the present phase which is much smaller than ~ 3.2 Å for the Sr-based $x=0$ phase. This value is close to Cu-O_{apical} lengths for typical 2D high-T_c cuprates. It indicates hybridization of Cu_{ladder} $3d$ and O_{chain} $2p$ orbitals. As a result, 30–50 % Cu atoms in the ladder sheet are coordinated pyramidally by five oxygen atoms including an apical oxygen atom belonging to the twisted 1D CuO_2 chain. The remaining Cu atoms are coordinated only by four O atoms within the ladder plane. This situation is illustrated in Fig. 13 where some of the Cu atoms in the ladder are coordinated by apical oxygen atoms belonging to upper or lower CuO_2 chain plane.

In the present system, the formal oxidation state of Cu is $+2.25$ if $\delta=0$. Holes are therefore ''self-doped'' in this solid solution. If the Cu_2O_3 ladder and CuO_2 chain sheets are not interacted, the holes enter preferably into CuO_2 chains, which are more electronegative than Cu_2O_3 planes.[52] However, shrinkage of the intersheet distance leads to redistribution of holes between them. Kato *et al.* suggested by bond-valence-sum calculations that holes are almost completely located at the 1D chain sites in $Sr_{14}Cu_{24}O_{41+\delta}$ and they move into ladder sites with increasing the Ca content.[38] After the Ca substitution, Osafune *et al.* found a transfer of the spectral weight from the high- to low-energy region in an optical conductivity spectrum. Based on this result they proposed the charge redistribution from the 1D chain site to the ladder one.[53] From Madelung potential calculations, Mizumo and co-workers have also concluded that holes are located on the 1D chain in the Sr-based phase and Ca substitution makes them move to the ladder.[54,55] The ladder subsystem is more
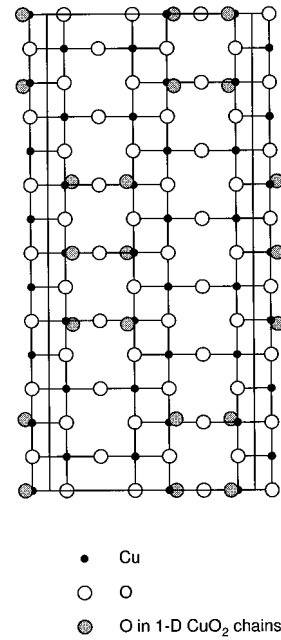

● Cu
○ O
◉ O in 1-D CuO_2 chains

FIG. 13. Arrangements of atoms in the ladder plane (Ref. 51). The shaded oxygen atoms of the upper or lower CuO_2 chains are bound to the Cu atoms of the ladder plane.

conductive than the 1D chain along the c axis since it has a larger transfer integral due to $\sim 180°$ Cu-O-Cu bond compared with $\sim 90°$ Cu-O-Cu bond in the 1D chain. Increase of electrical conductivity by Ca substitution can be, therefore, explained assuming the hole redistribution.

All above reports are consistent with the structural data of the present phase. For the five-coordinated Cu atom, Cu-O distances within the ladder plane are shortened substantially compared with the four-coordinated Cu atom[51] suggesting that holes are introduced into the antibonding Cu $3d$ and O $2p$ hybrid orbitals of the ladder plane. It is worth noting that such a five-coordinated Cu atom is placed side by side making a pair connected by a rung which is required by the symmetry of the crystal (see Fig. 13). It may be related to pairing of holes, i.e., spin-singlet superconductivity. Under high pressure, the interaction between the ladder and the 1D chain should be more pronounced because of the large shrinkage along the b axis. At $P=5$ GPa, for instance, the Cu_{ladder}-O_{apical} bondlength is roughly calculated as ~ 2.5 Å according to the present compressibility data. Under high pressure, therefore, the hole redistribution will be accelerated and hole density in the ladder is expected to increase. We believe that this is the most important role of high pressure for realizing superconductivity.

At ambient pressure, the $\rho - T$ curve shows a broad hump with two metal-semiconductor-like transitions near 160 and 50 K. This strange and characteristic behavior has been observed in samples with the Ca content $x \geq 13.0$. The second increase of the resistivity seems to be explained by localization of carriers due to random potential (see below). The first increase near 160 K reminds us of an incomplete Peierls-transition observed in a quasi-1D system such as $NbSe_3$.[56–59] The resistivity of $NbSe_3$ shows a downturn soon after the transition because of incomplete nesting of the Fermi surface owing to two-dimensional character in its electronic struc-

ture. For the present two-leg ladder system, the theory strongly suggests competition of the superconducting state and CDW state at low temperature. The first transition near 160 K may be attributed to the incomplete Peierls-transition. Based on this picture, the systematic suppression of the hump with increasing pressure may suggest enhancement of two-dimensional character under high pressure. Indeed, a recent single-crystal study indicated that resistivity along the a axis (rung direction) decreases substantially under high pressure and it becomes metallic even in a low-temperature region.[60] Here, we note variation of the a axis under high pressure. As described above, thermal shrinkage along the a axis is pronounced under high pressure (Fig. 9) and this behavior seems to be consistent with the metallic conductivity along the a axis under high pressure and low temperature. Also, it is interesting to compare the effects of the Ca substitution and pressure on the lattice. If only the carrier doping due to the b-axis shrinkage is important for superconductivity, even a less Ca-substituted sample may show superconductivity by applying higher pressure. However, $Sr_4Ca_{10}Cu_{24}O_{41+\delta}$ did not show superconductivity up to 8.5 GPa.[61] As shown in Table I, both the a and c axis shrink in nearly the same percentage after the Ca substitution, whereas pressure induces, in the high-temperature region, more anisotropic intraplane shrinkage with a larger percentage along the c axis than along the a axis. The Ca substitution seems, therefore, to enhance interladder interaction along the a axis. These facts suggest that superconductivity appears after the system has two-dimensional character.

Expecting direct observation of the Peierls transition, we carried out electron-diffraction measurements around 100 K, but no evidence for it was obtained. Even if there appear extra spots due to the charge order, it may be difficult to detect them in the present system because they would be overlapped with the satellite spots (including higher order reflections) of the composite lattice. In the temperature dependence of the b axis, however, we found an anomalous behavior near 150 K where the b axis does not change smoothly as a function of temperature, which cannot be interpreted using the classical Grüneisen's equation of state.[62] If there is really a breaking point, it means an abrupt change of the thermal-expansion coefficient and the presence of a second-order phase transition. This anomaly may correspond to the increase of resistivity near 160 K. We need, however, more detailed studies to clarify this point. In particular, the temperature variation of the phonon spectra will be helpful to observe the softening of the phonon.

The atomic arrangement in the ladder subsystem is largely modulated by the intersheet interaction. The random potential influences the carrier transport properties because of narrow energy bands of the low-dimensional system. In Fig. 14, we plotted low-temperature resistivity data of 0–5 GPa normalized at 30 K using the formula of the variable-range-hopping (VRH) scheme: $\rho \propto \exp[-(Q/T)^{1/(d+1)}]$, where Q is a parameter in proportion to inverse of density of states at Fermi-surface $N(E_F)$, and d is the dimensionality of the carrier conduction. The data could be well fitted assuming $d=3$ as shown in Fig. 14. However, the difference between the fittings with $d=3$ and $d=1$ or 2 was not statistically significant. We could not determine the dimensionality of the system by this method. The VRH conduction is explained by
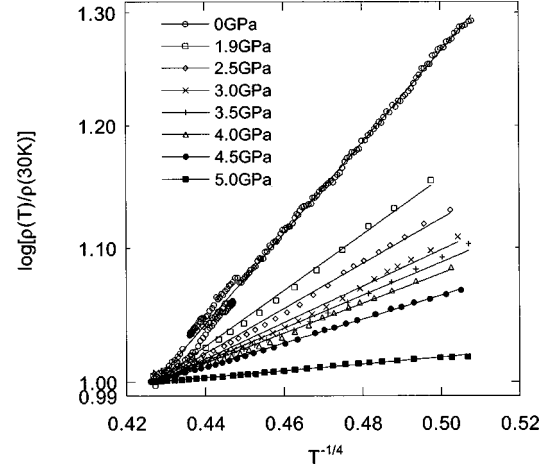

FIG. 14. Logarithmic resistivity $\ln[\rho(T)/\rho(30\ K)]$ plotted against $1/T^4$.

carrier transfer between localized states near the Fermi level via the phonon potential in a random field. In the fitting of Fig. 14, the slope decreases continuously with increasing pressure. This may suggest the evolution of an in-gap state and/or screening of the random potential by increasing hole density. Anyway, the carrier localization tends to be suppressed drastically with increasing pressure. When $P = 5$ GPa, the carrier localization vanishes and T_c takes the maximum. The enhancement of the superconductivity is attributed to an increase of hole density.

The reason for the suppression of the superconductivity in the metallic state above 5 GPa is not yet clear. To discuss the electronic structure in the metallic region, we fitted the resistivity data of 5–6 GPa using a power-law function of $\rho = \rho_0 + AT^n$ (ρ_0: residual resistivity). The results are shown in Fig. 15. The data are well fitted assuming n between 1 and ~ 2 over a wide temperature range at least up to ~ 200 K. Around 300 K, the $\rho(T)$ deviates from the power law with the constant n and obeys T-linear dependence. It should be noted that such a temperature dependence cannot be interpreted by the Bloch-Grüneisen (BG) theory which is based on the electron-phonon scattering.[62] In the BG theory, the exponent n changes from 5 to 1 within a narrow temperature
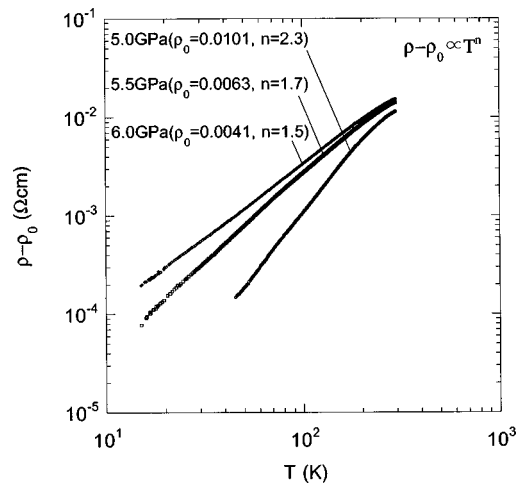

FIG. 15. A logarithmic plot of $(\rho - \rho_0)$ versus T for the data above 5 GPa.

range below Debye temperature θ_D: roughly speaking $n \sim 5$ for $T \sim 0$ and $n \sim 1$ for $T > 0.3\theta_D$. Hence, if one explains the data using the BG theory, an unreasonably high Debye temperature should be assumed.

Based on the fact that the resistivity obeys $\rho = \rho_0 + AT^2$, Uehara *et al.* have proposed the normal Fermi-liquid state for the present system under high pressure where superconductivity is realized.[40] Our data at 5 GPa seems to, roughly speaking, obey the T-square law, as well. This behavior is explained assuming that carriers are scattered mainly by spin fluctuations. The approach to the T-linear dependence from the T-square-like one near 300 K may be explained in terms of antiferromagnetic spin scattering using Fermi-liquid theories as well as that for 2D high-T_c cuprates.[63–65] According to the self-consistent renormalization theory, the $\rho(T)$ is proportional to $\sim \chi_{\mathbf{Q}=\pi}T^2 \sim T^2/(T_1 T) = T/T_1$ ($\chi_{\mathbf{Q}}$ is a staggered susceptibility, T_1 is a nuclear spin-lattice relaxation time). Since T_1 approaches to be constant with increasing temperature,[66] $\rho(T)$ is proportional to T at the high-temperature limit.

The exponent approaches to 1 from 2 as pressure increases. In addition, the T-dependent term in ρ increases with pressure. These are completely different from the tendency often observed in 2D high-T_c cuprates, in which the variation of resistivity changes gradually from T-linear to T-square-like with increasing carrier density, resulting in suppression of superconductivity.[67] Simple comparison of the present system with the 2D high-T_c cuprates seems difficult and suppression of superconductivity above 5 GPa is still open to question. We need to know the pairing mechanism for solving this problem. In addition, it seems important to know about the spin gap under high pressure.

V. CONCLUSIONS

We studied the x-ray diffraction and electrical resistivity in a composite crystal $Sr_{0.4}Ca_{13.6}Cu_{24}O_{41+\delta}$ under high pressure and low temperature to discuss the nature of the electronic state and pressure-induced superconductivity from crystallographic aspects. The $Sr_{0.4}Ca_{13.6}Cu_{24}O_{41+\delta}$ phase survives at least for $P \lesssim 9$ GPa and $T \gtrsim 7$ K indicating that it is responsible for superconductivity observed only under high pressure. High pressure and the Ca substitution lead to enhancement of the interaction between the Cu_2O_3 ladder and the 1D CuO_2 chain through shrinkage of the intersheet distance. Holes are doped into ladders from 1D chains via locally formed Cu_{ladder} $3d$ and O_{chain} $2p$ hybrid orbitals. An anomalous hump was observed in the ρ-T curve in a lower pressure region and is possibly due to the CDW. Carrier localization observed at low temperature is explained by a random potential in the modulated ladder structure. It is suppressed drastically with increasing pressure. The ρ-T curves in the normal state above 5 GPa obey a power law of temperature in the wide range of temperature between 7 and over 200 K, suggesting that carriers are mainly scattered by spin fluctuation as well as in 2D high-T_c cuprates. T_c increases up to ~ 13 K at 5 GPa, and then is suppressed in the metallic state above 5 GPa. The reason for the suppression is not clear yet.

*Permanent address: National Laboratory for Superconductivity, Institute of Physics, Chinese Academy of Sciences, Beijing, China.

[1] E. Dagotto, J. Riera, and D. Scalapino, Phys. Rev. B **45**, 5744 (1992).

[2] D. C. Johnston, J. W. Johnson, D. P. Goshorn, and A. P. Jacobson, Phys. Rev. B **35**, 219 (1987).

[3] R. S. Eccleston, T. Bernes, J. Brody, and J. W. Johnson, Phys. Rev. Lett. **73**, 2626 (1994).

[4] Y. Furukawa, A. Iwai, K. Kumagai, and A. Yakubovski, J. Phys. Soc. Jpn. **65**, 2393 (1996).

[5] Z. Hiroi, M. Azuma, M. Takano, and Y. Bando, J. Solid State Chem. **95**, 230 (1991).

[6] M. Azuma, Z. Hiroi, M. Takano, K. Ishida, and Y. Kitaoka, Phys. Rev. Lett. **73**, 3463 (1994).

[7] K. Ishida, Y. Kitaoka, K. Asayama, M. Azuma, Z. Hiroi, and M. Takano, J. Phys. Soc. Jpn. **63**, 3222 (1994).

[8] T. Barnes, E. Dagotto, J. Riera, and E. S. Swanson, Phys. Rev. B **47**, 3196 (1993).

[9] T. M. Rice, S. Gopalan, and M. Siegrist, Physica B **199&200**, 378 (1994).

[10] S. Gopalan, T. M. Rice, and M. Siegrist, Phys. Rev. B **49**, 8901 (1994).

[11] M. Siegrist, T. M. Rice, and F. C. Zhang, Phys. Rev. B **49**, 12 058 (1994).

[12] H. Tsunetsugu, M. Troyer, and T. M. Rice, Phys. Rev. B **49**, 16 078 (1994).

[13] R. M. Noack, S. R. White, and D. J. Scalapino, Phys. Rev. Lett. **73**, 882 (1994).

[14] M. Troyer, H. Tsunetsugu, and D. Wurtz, Phys. Rev. B **50**, 13 515 (1994).

[15] H. Tsunetsugu, M. Troyer, and T. M. Rice, Phys. Rev. B **51**, 16 456 (1995).

[16] C. A. Hayward, D. Poilblanc, R. M. Noack, D. J. Scalapino, and W. Hanke, Phys. Rev. Lett. **75**, 926 (1995).

[17] D. J. Scalapino, Nature (London) **377**, 12 (1995).

[18] E. Dagotto and T. M. Rice, Science **271**, 618 (1996).

[19] C. A. Hayward, D. Poilblanc, and D. J. Scalapino, Phys. Rev. B **53**, R8863 (1996).

[20] C. A. Hayward and D. Poilblanc, Phys. Rev. B **53**, 11 721 (1996).

[21] K. Sano, J. Phys. Soc. Jpn. **65**, 1146 (1996).

[22] V. J. Emery and S. A. Kivelson, Physica C **209**, 597 (1993).

[23] Z. Hiroi and M. Takano, Nature (London) **377**, 41 (1995).

[24] Z. Hiroi, J. Solid State Chem. **123**, 223 (1996).

[25] M. Takano, Physica C **263**, 468 (1996).

[26] K. Kato, E. Takayama-muromachi, K. Kosuda, and Y. Uchida, Acta Crystallogr., Sect. C: Cryst. Struct. Commun. **44**, 1881 (1988).

[27] K. Kato, Acta Crystallogr., Sect. B: Struct. Sci. **46**, 39 (1990).

[28] E. M. McCarron III, M. A. Subramanian, J. C. Calabrese, and R. L. Harlow, Mater. Res. Bull. **23**, 1355 (1988).

[29] T. Siegrist, L. F. Schneemeyer, S. A. Sunshine, and J. V. Waszczak, and R. S. Roth, Mater. Res. Bull. **23**, 1429 (1988).

[30] K. Ukei, T. Shishido, and T. Fukuda, Acta Crystallogr., Sect. B: Struct. Sci. **50**, 42 (1994).

[31] A. F. Jensen, F. K. Larsen, B. B. Iversen, V. Petricek, T. Schultz, and Y. Gao, Acta Crystallogr., Sect. B: Struct. Sci. **53**, 113 (1997).

[32] A. F. Jensen, V. Petricek, F. K. Larsen, and E. M. McCarron III, Acta Crystallogr., Sect. B: Struct. Sci. **53**, 125 (1997).

[33] M. Matsuda and K. Katsumata, Phys. Rev. B **53**, 12 201 (1996).

[34] M. Matsuda, K. Katsumata, H. Eisaki, N. Motoyama, and S. Uchida, Phys. Rev. B **54**, 12 199 (1996).

[35] R. S. Eccleston, M. Azuma, and M. Takano, Phys. Rev. B **53**, R14 721 (1996).

[36] H. Yamane, Y. Miyazaki, and H. Hirai, J. Ceram. Soc. Jpn. **98**, 1050 (1990).

[37] M. Kato, H. Chizawa, Y. Koike, T. Noji, and Y. Saito, Physica C **235-240**, 1327 (1994).

[38] M. Kato, K. Shiota, and Y. Koike, Physica C **258**, 284 (1996).

[39] M. Kato, K. Shiota, S. Ikeda, Y. Maeno, T. Fujita, and Y. Koike, Physica C **263**, 482 (1996).

[40] M. Uehara, T. Nagata, J. Akimitsu, H. Takahashi, N. Môri, and K. Kinoshita, J. Phys. Soc. Jpn. **65**, 2764 (1996).

[41] D. N. Batchelder and O. Simmons, J. Chem. Phys. **41**, 2324 (1964).

[42] H. K. Mao, P. M. Bell, J. W. Shaner, and D. J. Steinberg, J. Appl. Phys. **49**, 3276 (1978).

[43] D. L. Decker, J. Appl. Phys. **42**, 3239 (1971).

[44] J. Tang, T. Matsumoto, and N. Môri, Rigaku-Denki J. **27**, 4 (1996), in Japanese.

[45] Y. Matsui, S. Horiuch, Y. Bando, Y. Kitami, M. Yokoyama, S. Suehara, I. Matsui, and T. Katsuta, Ultramicroscopy **39**, 8 (1991).

[46] X.-J. Wu, E. Takayama-Muromachi, S. Suehara, and S. Horiuch, Acta Crystallogr., Sect. A: Found. Crystallogr. **47**, 727 (1991).

[47] X.-J. Wu and S. Horiuch, Acta Crystallogr., Sect. A: Found. Crystallogr. **47**, 11 (1991).

[48] O. Milat, G. Van Tendeloo, and S. Amelinckx, Acta Crystallogr., Sect. A: Found. Crystallogr. **48**, 618 (1992).

[49] A. Yamamoto, Acta Crystallogr., Sect. A: Cryst. Phys., Diffr., Theor. Gen. Crystallogr. **38**, 87 (1982).

[50] A. Yamamoto, Acta Crystallogr., Sect. A: Found. Crystallogr. **48**, 476 (1992).

[51] T. Ohta, M. Onoda, F. Izumi, M. Isobe, E. Takayama-Muromachi, and A. W. Hewat, J. Phys. Soc. Jpn. **66**, 3107 (1997).

[52] S. A. Carter, B. Batlogg, R. J. Cava, J. J. Krajewski, W. F. Peck, Jr., and T. M. Rice, Phys. Rev. Lett. **77**, 1378 (1996).

[53] T. Osafune, N. Motoyama, H. Eisaki, and S. Uchida, Phys. Rev. Lett. **78**, 1980 (1997).

[54] Y. Mizuno, T. Thoyama, and S. Maekawa, J. Phys. Soc. Jpn. **66**, 937 (1997).

[55] Y. Mizuno, T. Thoyama, and S. Maekawa, Physica C **282−287**, 991 (1997).

[56] P. Monceau, N. P. Ong, A. M. Portis, A. Meerschaut, and J. Rouxel, Phys. Rev. Lett. **37**, 602 (1976).

[57] N. P. Ong, Phys. Rev. B **17**, 3243 (1978).

[58] R. M. Fleming and C. C. Grimes, Phys. Rev. Lett. **42**, 1423 (1979).

[59] K. Tsutsumi, T. Takagi, M. Yamamoto, Y. Shiozaki, M. Ido, T. Sambongi, K. Yamaya, and Y. Abe, Phys. Rev. Lett. **39**, 1675 (1977).

[60] T. Nagata *et al.*, in *Meeting Abstracts of the Physical Society of Japan*, Vol. 52, Issue 1, Part 3 (Nihon-Butsuri-Gakkai, Tokyo, 1997), p. 649 (in Japanese).

[61] N. Môri, H. Takahashi, and T. Nakanishi, in *Solid State Physics* (Agne-Gijutsu-Center, Tokyo, 1996), Vol. 31, p. 797 (in Japanese).

[62] See, e.g., J. M. Ziman, in *Principles of the Theory of Solids*, 2nd ed. (Maruzen, Tokyo, 1985) (in Japanese).

[63] T. Moriya, T. Takahashi, and K. Ueda, J. Phys. Soc. Jpn. **59**, 2905 (1990).

[64] H. Kohno and K. Yamada, Prog. Theor. Phys. **85**, 13 (1991).

[65] K. Yamada, in *Magnetism and Superconductivity in Itinerant Electron Systems*, edited by A. Kawabata and H. Yasuoka (Shokabo, Tokyo, 1992), p. 16 (in Japanese).

[66] K. Magishi, S. Matsumoto, K. Ishida, Y. Kitaoka, K. Asayama, M. Uehara, T. Nagata, and J. Akimitsu, Physica C **282−287**, 1115 (1997).

[67] Y. Kubo, Y. Shimakawa, T. Manako, and H. Igarashi, Phys. Rev. B **43**, 7875 (1991).